Journal of Energy Storage 141 (2026) 119425

Contents lists available at ScienceDirect

Journal of Energy Storage

journal homepage: www.elsevier.com/locate/est

Research Papers

Enhancing potential window with ionic liquid/water in salt mixture in co-doped activated carbon electrodes for high-energy supercapacitors

S. Thior [a], V.N. Kitenge [a], Ndeye F. Diop [a], Kabir O. Otun [a], V.M. Maphiri [a], Rashed A.M. Adam [a], Balla D. Ngom [b], N. Manyala [a,*]

[a] Department of Physics, Institute of Applied Materials, SARChI Chair in Carbon Technology and Materials, University of Pretoria, Pretoria, 0002, South Africa
[b] Laboratoire de Photonique Quantique, d'Energie et de Nano-Fabrication, Faculté des Sciences et Techniques, Université Cheikh Anta Diop de Dakar (UCAD), B.P. 5005, Dakar-Fann Dakar, Senegal

ARTICLE INFO

Keywords:
Water in salt
12 m $NaNO_3$
Ionic liquid
EMIM DCA
Mixture electrolyte
Supercapacitor

ABSTRACT

This study presents a novel electrolyte system combining 1-ethyl-3-methylimidazolium dicyanamide (EMIM DCA) with 12 m sodium nitrate ($NaNO_3$) to optimize ionic interactions for advanced supercapacitor performance. Maintaining a constant EMIM DCA concentration, $NaNO_3$ was varied to yield molar ratios of [EMIM DCA]$_1$[12 m $NaNO_3$]$_1$, [EMIM DCA]$_1$[12 m $NaNO_3$]$_2$, and [EMIM DCA]$_1$ [12 m $NaNO_3$]$_3$. The resulting mixtures were rigorously characterized for viscosity, density, ionic conductivity, and molecular interactions using Fourier-transform infrared (FTIR) and Raman spectroscopy. Electrochemical evaluation in a three-electrode configuration at 0.5 A g^{-1}, employing nitrogen and sulfur co-doped activated carbon (N,S-AC) electrodes, revealed a maximum specific capacitance of 257 F g^{-1} for the [EMIM DCA]$_1$[12 m $NaNO_3$]$_1$ composition, significantly surpassing the performance of pure $NaNO_3$. When implemented in a symmetric supercapacitor operating at 2.3 V, this electrolyte achieved a specific energy of 50.22 Wh kg^{-1} and a power density of 583.97 W kg^{-1} at 0.5 A g^{-1}, with 83.33 % capacitance retention after 10,000 charge-discharge cycles. These results underscore the [EMIM DCA]$_1$[12 m $NaNO_3$]$_1$ electrolyte as a high-performance, cost-effective solution for durable supercapacitors, offering substantial potential for applications in renewable energy storage and electric vehicle power systems with further tuning of water in salt-based electrolytes.

1. Introduction

To address the accelerating global demand for energy, electrochemical energy storage technologies, particularly supercapacitors, have gained prominence due to their exceptional capacity for rapid power delivery [1–3]. However, their limited energy density poses a critical challenge, restricting their suitability for specific energy storage applications. Enhancing energy density while preserving high power density and long-term cycle stability is imperative to broaden the practical applicability of supercapacitors in advanced energy storage technologies [4,5]. The energy density of supercapacitors, governed by the equation $E = ½ CV^2$, is predominantly determined by the specific capacitance (C) and the operational voltage window (V). The capacitance is intricately dependent on the physicochemical properties of both electrode and electrolyte materials, whereas the voltage window is primarily dictated by the electrolyte's electrochemical stability. Given the quadratic relationship between energy density and voltage, expanding the voltage window significantly enhances energy storage capacity. Consequently, developing electrolytes with a broad electrochemical stability window is critical for optimizing supercapacitor performance and advancing their utility in high-energy-density applications [6]. The electrolyte constitutes a critical element in supercapacitor systems, exerting a profound influence on ionic conductivity, electrochemical stability, and energy density efficiency, thereby playing a central role in determining the overall performance and efficacy of these energy storage devices [7]. Aqueous electrolytes typically exhibit a limited electrochemical stability window due to water electrolysis, which initiates at 1.23 V, constraining their voltage range in supercapacitor applications [8]. Nevertheless, organic electrolytes are flammable, volatile, and poisonous, with high viscosity and low ionic conductivity [9]. To overcome the constraints of conventional electrolytes, water-in-salt electrolytes (WiSE) have emerged as a highly promising alternative. Initially reported by Suo et al. in 2015, these electrolytes feature a salt concentration exceeding that of the solvent in

* Corresponding author.
E-mail address: ncholu.manyala@up.ac.za (N. Manyala).

https://doi.org/10.1016/j.est.2025.119425
Received 7 August 2025; Received in revised form 13 October 2025; Accepted 6 November 2025
Available online 11 November 2025

both mass and volume, significantly expanding the electrochemical stability window. This enables supercapacitors to operate at elevated voltages, thereby substantially improving energy and power densities for advanced energy storage applications [10,11]. Despite their potential, water-in-salt electrolytes encounter significant challenges, including reduced ionic conductivity and compromised wettability stemming from near-saturated salt concentrations, which restrict the electrochemically active surface area. Additionally, the risk of salt precipitation due to solubility variations can impair the rate performance of electric double-layer capacitor (EDLC) supercapacitors, limiting their overall efficacy in high-performance energy storage applications [12]. To enhance supercapacitor performance, further refinement of electrolyte systems is imperative. To address the limitations of water-in-salt electrolytes, researchers have developed hybrid electrolyte systems that integrate organic or ionic liquid co-solvents with aqueous water-in-salt solutions. For instance, Qingyun Dou et al. explored a hybrid organic-water-in-salt electrolyte comprising acetonitrile and a 5 M lithium bis(trifluoromethanesulfonyl)imide (LiTFSI) aqueous solution. Their findings revealed significant enhancements in energy and power density compared to the standalone 5 M LiTFSI electrolyte. Specifically, the hybrid system achieved a specific capacitance of 108 F g^{-1} at a current density of 1 A g^{-1}, underscoring its potential to advance the efficiency and applicability of supercapacitors in high-performance energy storage technologies [13]. A parallel investigation by Quindund et al. explored a hybrid water-in-salt electrolyte incorporating an ionic liquid (LiTFSI-EMIM TFSI), achieving an expanded electrochemical stability window of 2.8 V. Their findings, derived from galvanostatic charge-discharge (GCD) measurements, revealed a specific capacity of 38 mA h g^{-1}, alongside notable energy and power densities metrics of 51.9 W h kg^{-1} at 0.37 kW kg^{-1}, evaluated at a current density of 0.5 A g^{-1}, highlighting the potential of such hybrid electrolytes for high-performance energy storage systems [14]. Schuurman et al. conducted a comprehensive study on a hybrid electrolyte system combining an ionic liquid with an aqueous component, tailored for supercapacitor applications. Their supercapacitor cell exhibited a specific capacitance of 136 F g^{-1} and a specific energy of 22 Wh kg^{-1}, highlighting the potential of such hybrid systems to enhance electrochemical performance in advanced energy storage devices [15]. Despite these improvements, the specific capacitance or capacity remained lower than expected for high-performance supercapacitors. This study presents an innovative strategy that integrates the attributes of a 12 m sodium nitrate ($NaNO_3$) water-in-salt electrolyte with the hydrophilic ionic liquid 1-ethyl-3-methylimidazolium dicyanamide (EMIM DCA) to advance supercapacitor performance. Both components were selected for their distinct electrochemical advantages. The 12 m $NaNO_3$ electrolyte exhibits superior ionic conductivity and exceptional electrochemical stability, positioning it as a compelling candidate for diverse electrochemical energy storage systems. Conversely, EMIM DCA, an imidazolium-based ionic liquid, is distinguished by its notably low viscosity relative to traditional ionic liquids, enhancing its suitability for efficient ion transport in high-performance applications [16,17]. The integration of EMIM DCA into water-in-salt (WiSE) electrolyte systems has proven to be an effective strategy for enhancing ion transport dynamics and extending electrochemical stability. Owing to its favorable physicochemical characteristics including high ionic conductivity, low volatility, and thermal resilience EMIM DCA contributes significantly to broadening the electrolyte's operating temperature range and stabilizing the overall system. To evaluate the electrochemical performance of this hybrid system, a series of ternary mixtures were prepared with varying molar ratios: [EMIM DCA]$_1$[12 m $NaNO_3$]$_1$, [EMIM DCA]$_1$[12 m $NaNO_3$]$_2$, and [EMIM DCA]$_1$[12 m $NaNO_3$]$_3$. These were characterized through viscosity, density, ionic conductivity, Fourier-transform infrared spectroscopy (FTIR) and Raman spectroscopy, followed by detailed electrochemical testing via cyclic voltammetry (CV), electrochemical impedance spectroscopy (EIS), and galvanostatic charge–discharge (GCD). Spectroscopic analysis revealed that the equimolar composition, [EMIM DCA]$_1$[12 m $NaNO_3$]$_1$, promotes stable molecular interactions within the electrolyte matrix, resulting in an extended electrochemical stability window (ESW) of 2.3 V. Electrochemical evaluation of the supercapacitor assembled with this optimal electrolyte demonstrated a high specific capacitance of 257 F g^{-1}. Furthermore, it achieved an energy density of 50.2 W h kg^{-1} and a power density of 583.97 W kg^{-1} at a current density of 0.5 A g^{-1}. Long-term cycling tests affirmed the system's robustness, with 83.33 % capacitance retention after 10,000 cycles at 5 A g^{-1} and a high Coulombic efficiency of 99.66 %. These results confirm the synergistic effect between EMIM DCA and highly concentrated $NaNO_3$, where the ionic liquid modulates the solvation environment, enhances ionic mobility, and stabilizes the electrode–electrolyte interface. The hybrid electrolyte [EMIM DCA]$_1$[12 m $NaNO_3$]$_1$ thus emerges as a promising candidate for next-generation high-performance supercapacitors, offering a balanced profile of high energy, power capability, and cycling durability.

2. Experimental method

2.1. Materials synthesis

The N,S-AC electrode, employed for the fabrication of supercapacitor electrodes, was synthesized via a single-step carbonization and activation process, as adapted from the methodology outlined by Kitenge et al. [16]. The hydrophilic ionic liquid 1-ethyl-3-methylimidazolium dicyanamide (EMIM DCA, $H_2O < 20$ ppm, 99.9 % purity) was sourced from Solvonic (Toulouse, France). Sodium nitrate ($NaNO_3$) was obtained from LABCHEM (South Africa). A 12 molal (m) sodium nitrate ($NaNO_3$) solution was prepared using deionized water as the solvent. Binary electrolyte mixtures, formulated with a fixed quantity of 1-ethyl-3-methylimidazolium dicyanamide (EMIM DCA) and varying molar ratios of $NaNO_3$, denoted as [EMIM DCA]$_1$[12 m $NaNO_3$]$_X$ (where x represents the molar ratio of $NaNO_3$), were synthesized by magnetic stirring at 120 rpm for 1 h. This process was conducted in an inert glovebox (Inert Technologies, USA) under a strictly controlled oxygen and water-free environment (0.0 % levels) to ensure the purity and stability of the electrolyte formulations. Three distinct electrolyte compositions were prepared: (1) [EMIM DCA]$_1$[12 m $NaNO_3$]$_3$, (2) [EMIM DCA]$_1$[12 m $NaNO_3$]$_2$, and (3) [EMIM DCA]$_1$[12 m $NaNO_3$]$_1$.

2.2. Characterization methods for electrolyte analysis

To establish the physicochemical and structural characteristics of the prepared electrolytes, a series of complementary analytical techniques were employed. The ionic conductivity of 12 m $NaNO_3$, EMIM DCA, and their hybrid mixtures was determined using a Jenco 3020 M conductivity meter (Jenco, USA) with a precision of ±0.5 μS cm^{-1}. All measurements were performed at 22.3 °C. The viscosity of the electrolytes was evaluated using an NDJ-8S RV digital viscometer (W & J Instrument Co., China). Each sample was equilibrated at room temperature before testing, and multiple readings were taken to confirm consistency. The density was measured with a Sigma 700 densimeter (Attension, KSV Instruments, Finland), providing essential information to correlate the bulk physicochemical properties with ionic transport behavior. To further elucidate molecular interactions within the mixtures, Fourier-transform infrared (FTIR) spectroscopy was carried out using a Varian 680-IR spectrometer (USA) over the range of 400–4000 cm^{-1}. Each spectrum was recorded after background correction, and repeated scans were performed to enhance spectral clarity. Complementary vibrational analysis was performed by Raman spectroscopy using a WITec Alpha 300 RAS+ confocal Raman microscope (WITec, Germany) equipped with a 523 nm excitation laser operating at 4 mW. Spectra were collected with an acquisition time of 120 s to achieve high signal intensity and well-resolved peaks.

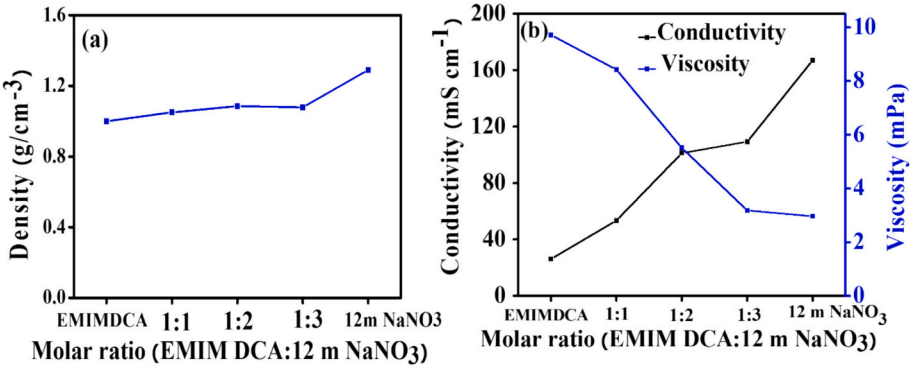

Fig. 1. (a) Conductivity and viscosity and (b) density measurements of 12 m $NaNO_3$, EMIM DCA, and (EMIM DCA: 12 m $NaNO_3$) electrolyte mixture, respectively.

2.3. Electrochemical techniques and calculations

The working electrode was fabricated by combining 80 % nitrogen and sulfur co-doped activated carbon (N,S-AC) as the active material, 10 % polyvinylidene fluoride (PVDF) as the binder, and 10 % conductive carbon black. The total mass loading of the electrode was 3 mg cm^{-2}. A slurry was prepared by homogenizing the mixture in *N*-methyl-2-pyrrolidone (NMP) and uniformly coating it onto both sides of a 1 × 1 cm^2 nickel foam substrate. The coated electrodes were dried in an oven at 60 °C for 12 h to ensure component adhesion. Electrochemical performance was evaluated using both three and two electrode configurations with a Biologic VMP 300 Potentiostat (USA) and analyzed via EC-Lab V11.50 software. In the three-electrode setup, a T-cell configuration was employed, with the N,S-AC-coated nickel foam as the working electrode, a silver (Ag/Ag^+) disc as the reference electrode, and mangosteen-derived activated carbon as the counter electrode. The active material mass was set to 3 mg cm^{-2}. All T-cells, except those using the aqueous 12 m $NaNO_3$ electrolyte, were assembled in the glovebox to maintain an inert environment. Cyclic voltammetry (CV) was conducted at scan rates of 5, 10, 20, 30, 40, 50, and 100 mV s^{-1} within potential windows of −1.3 to 0.0 V for the negative electrode and 0.0 to 1.0 V for the positive electrode, referenced to the Ag/Ag^+ electrode. Galvanostatic charge-discharge (GCD) tests were performed at specific currents of 0.5, 1, 2, 3, 4, 5, and 10 A g^{-1} for both electrodes. Electrochemical impedance spectroscopy (EIS) was carried out over a frequency range of 10 mHz to 100 kHz at open-circuit potential. For the symmetric supercapacitor, a T-cell was assembled with two identical N,S-AC electrodes separated by a filter paper membrane and soaked in an electrolyte mixture of $[EMIM\ DCA]_1[12\ m\ NaNO_3]_1$. CV measurements were conducted at various scan rates with a voltage window of 0 to 2.3 V, and GCD tests were performed at specific currents of 0.5, 1, 2, 3, 4, and 5 A g^{-1} within the same voltage range. Specific capacitances in the three-electrode configuration were calculated from the GCD curves using the appropriate equation for discharge characteristics [17]:

$$C_{sp}\ (\text{three}) = \frac{I\Delta t}{\text{m}\Delta \text{v}}\left(\text{F g}^{-1}\right) \tag{1}$$

In this equation, I, Δt, m, and ΔV represent the applied current, discharge time, electrode mass, and potential window, during the discharge process, respectively.

The single-electrode capacitance (C_{SP}), energy density (E_{SP}), power density (P_{SP}), and coulombic efficiency (ŋ) of the two-electrode system were calculated from the GCD profiles using the following equations [18]:

$$C_{SP\ single\ (two)} = \frac{4I\Delta t}{M\Delta V}\left(\text{F g}^{-1}\right) \tag{2}$$

$$E_{SP} = \frac{C_{SP\ single\ (two)}\Delta V^2}{28.8}\left(\text{Wh kg}^{-1}\right) \tag{3}$$

$$P_{SP} = 3600 \times \frac{E_{SP}}{\Delta t}\left(\text{Wkg}^{-1}\right) \tag{4}$$

$$\text{ŋ} = \frac{\Delta t_{discharge}}{\Delta t_{charge}} \times 100(\%) \tag{5}$$

Here, M represents the total mass of both electrodes, I is the applied current, Δt is the discharge time, and ΔV is the voltage of the device.

To maintain charge balance within the device, a mass balance equation is essential, given the differences in working potential and charge-discharge time between the positive and negative electrodes. Consequently, the following equation was applied to achieve charge balance [8,19].

$$\frac{m_+}{m_-} = \frac{C_{S-}\Delta V_-}{C_{S+}\Delta V_+} \tag{6}$$

3. Results and discussion

3.1. Electrolyte characterization

This study investigates a series of binary hybrid electrolytes formulated by combining 1-ethyl-3-methylimidazolium dicyanamide (EMIM DCA) with an aqueous 12 molal (m) sodium nitrate ($NaNO_3$) solution to evaluate the effect of salt concentration on their physicochemical and electrochemical properties. A constant volume of 10 mL of EMIM DCA was used across all formulations, with its molar quantity determined from its density and molar mass. The $NaNO_3$ content was varied to achieve molar ratios of $[EMIM\ DCA]_1[12\ m\ NaNO_3]_1$, $[EMIM\ DCA]_1[12\ m\ NaNO_3]_2$, and $[EMIM\ DCA]_1[12\ m\ NaNO_3]_3$. Mole fractions were calculated to enable precise comparisons across compositions. Density, viscosity, and ionic conductivity were measured using established densimetric, viscometric, and conductivity techniques to assess the influence of $NaNO_3$ concentration. As expected, the density of the electrolyte mixtures increased with higher $NaNO_3$ content, consistent with the higher density of the 12 m $NaNO_3$ solution (~1.29 g cm^{-3}) compared to EMIM DCA (~0.98 g cm^{-3}), as shown in Fig. 1(a). However, at the 1:3 molar ratio of EMIM DCA to $NaNO_3$, a slight decrease in density was observed. This behavior can be explained by the presence of specific ion–solvent interactions that weaken the overall electrostatic forces within the system, resembling the effect observed in ionic liquids, where tuning the charge distribution results in a reduction in density. In the present mixture, $EMIM^+$ and DCA^- ions likely perturb the packing of Na^+–NO_3^- hydration shells, slightly expanding the local structure and reducing the overall density. This non-ideal mixing reflects the complex interplay of solvation, ion pairing, and molecular packing in determining bulk properties of ionic liquid–salt aqueous systems [20]. The $[EMIM\ DCA]_1[NaNO_3]_3$ mixture exhibited the lowest viscosity at 3.18 mPa s, followed by 5.51 mPa s for $[EMIM\ DCA]_1[12\ m\ NaNO_3]_2$, and 8.42 mPa s for $[EMIM\ DCA]_1[12\ m\ NaNO_3]_1$ as seen in Fig. 1(b). This

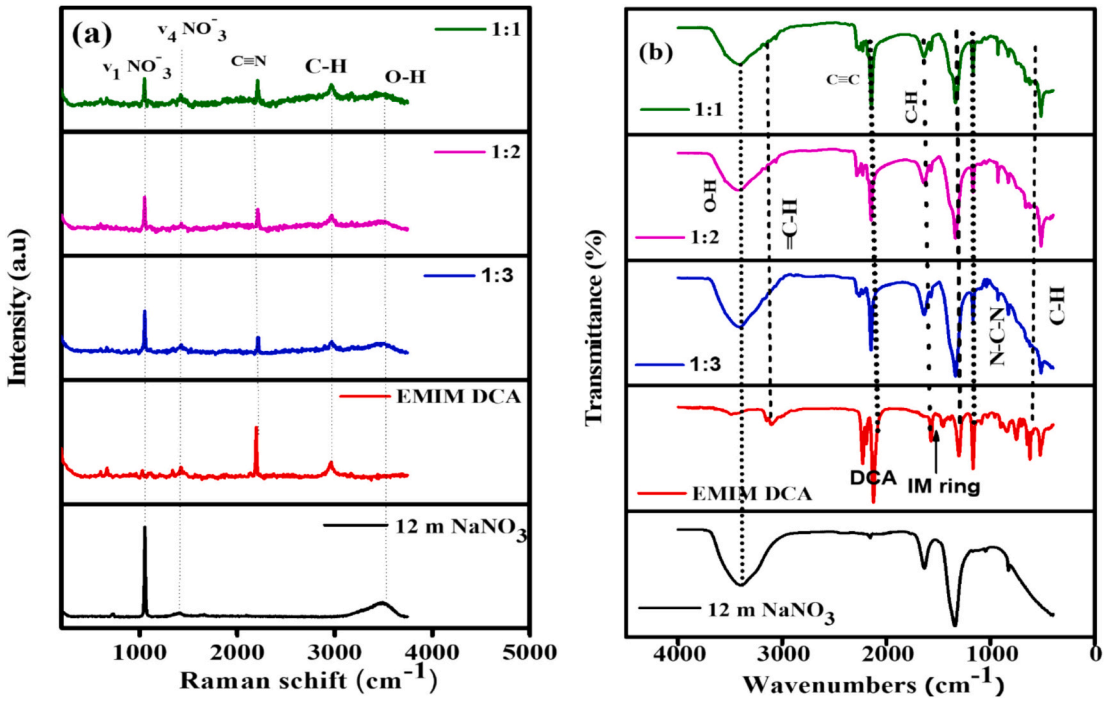

Fig. 2. Spectroscopic characterization of EMIM DCA, 12 m $NaNO_3$, and their binary mixtures ($[EMIM\ DCA]_1[12\ m\ NaNO_3]_X$, x = 1, 2, 3): (a) Raman spectra and (b) FTIR spectra.

reduction in viscosity is attributed to the dilution of the viscous ionic liquid by the aqueous $NaNO_3$ phase, which weakens coulombic interactions and enhances ion mobility [20]. The ionic conductivity of the hybrid electrolyte was strongly governed by the amount of $NaNO_3$ present. The ionic conductivity exhibited a gradual and consistent enhancement as the salt concentration increased. Among the different formulations, the $[EMIM\ DCA]_1[NaNO_3]_3$ mixture exhibited the highest value, reaching 109 mS·cm^{-1}, compared with 53.3 mS·cm^{-1} and 102 mS·cm^{-1} for the $[EMIM\ DCA]_1[12\ m\ NaNO_3]_1$ and $[EMIM\ DCA]_1[12\ m\ NaNO_3]_2$ compositions, respectively, as illustrated in Fig. 1(b). This steady enhancement in conductivity with greater salt loading can be understood in terms of two interrelated factors: Improved dissociation of ions and enhanced mobility of charge carriers. At elevated $NaNO_3$ concentrations, the larger population of Na^+ and NO_3^- ions more effectively disrupt ionic aggregates and breaks down water clusters, thereby creating an environment where ions move more freely and transport becomes faster. In addition to this concentration effect, the conductivity gain also reflects changes in the local solvation structure. At higher salt contents, Na^+ ions establish compact solvation shells through strong coordination with water and favorable pairing with nitrate anions. Such interactions weaken the extended hydrogen-bonding network typical of bulk water, thereby limiting the formation of larger water clusters that would otherwise restrict ion transport. By reorganizing the solvation landscape in this way, the concentrated mixtures promote a more dynamic medium that supports efficient ionic movement.

Raman and FTIR spectroscopy were used to clarify the molecular interactions and structural changes that occur when 1-ethyl-3-methylimidazolium dicyanamide (EMIM DCA) is combined with concentrated aqueous sodium nitrate (12 m $NaNO_3$). Measurements were performed for the individual components as well as for their mixtures ($[EMIM\ DCA]_1[12\ m\ NaNO_3]_X$, x = 1, 2, 3). In the Raman spectrum of pure $NaNO_3$ (Fig. 2(a)), a broad feature at ~3335 cm^{-1} corresponds to O—H stretching vibrations from extended hydrogen-bonded water clusters. When EMIM DCA is introduced, this band shifts progressively to higher frequencies (3447–3503 cm^{-1}) and decreases in intensity. The shift to higher wavenumbers reflects a weakening of water–water hydrogen bonding as Na^+ ions form compact hydration shells and compete with bulk water for coordination. At the same time, $EMIM^+$ cations interact with water through hydrogen bonding, further destabilizing extended networks. These changes reduce the amount of free water in the system, which directly suppresses hydrogen and oxygen evolution reactions. As a result, the electrolyte exhibits improved interfacial stability and an expanded electrochemical window compared to conventional aqueous systems. Characteristic Raman bands of EMIM DCA appear at 2220 cm^{-1} (C≡N stretching of DCA^-) and 2936 cm^{-1} (C—H stretching of $EMIM^+$). In the mixed electrolytes, the C≡N vibration downshifts to 2216 cm^{-1}, while the C—H band shifts to ~2989 cm^{-1}. The downshift of the C≡N band indicates stronger coordination between DCA^- and solvated cations (Na^+ and $EMIM^+$), confirming the formation of compact ion-paired structures. Such solvation restructuring reduces the energy required for desolvation during charge transfer, thereby accelerating ionic transport. The appearance of additional bands at ~1054 and 1386 cm^{-1}, assigned to symmetric (ν_1) and asymmetric (ν_4) stretching of NO_3^-, highlights the active role of nitrate in the reorganized solvation environment.

FTIR spectroscopy provides further evidence of this reorganization (Fig. 2(b)). The O—H band of aqueous $NaNO_3$ at ~3335 cm^{-1} shifts to higher wavenumbers and broadens in the mixtures, again indicating the breakdown of bulk hydrogen-bonded clusters. Pure EMIM DCA exhibits distinct peaks at 2127 cm^{-1} (C≡N stretching), 1343 cm^{-1} (N–C–N bending of DCA^-), and several imidazolium ring vibrations at 1573, 1163, and 620 cm^{-1} [21,22]. In the mixed electrolytes, these bands shift to 2216 cm^{-1} and ~ 2989 cm^{-1}, respectively. The red-shift of the C≡N mode suggests stronger electrostatic interactions between DCA^- and solvated Na^+ species, while the C—H shift indicates altered hydrogen-bonding interactions involving $EMIM^+$. These changes confirm that both cation-anion and ion-solvent interactions are reorganized in the mixed system, giving rise to a more compact and stabilized solvation structure. Such structural rearrangements improve interfacial stability by minimizing side reactions between water and the electrode surface and by facilitating the formation of desolvated or partially solvated ions that can more easily penetrate sub-nanometer pores of carbon electrodes. Additional new bands observed at 1054 cm^{-1} and 1386 cm^{-1} correspond to symmetric (ν_1) and asymmetric (ν_4) NO_3^- stretching, further confirming the active participation of nitrate anions in the

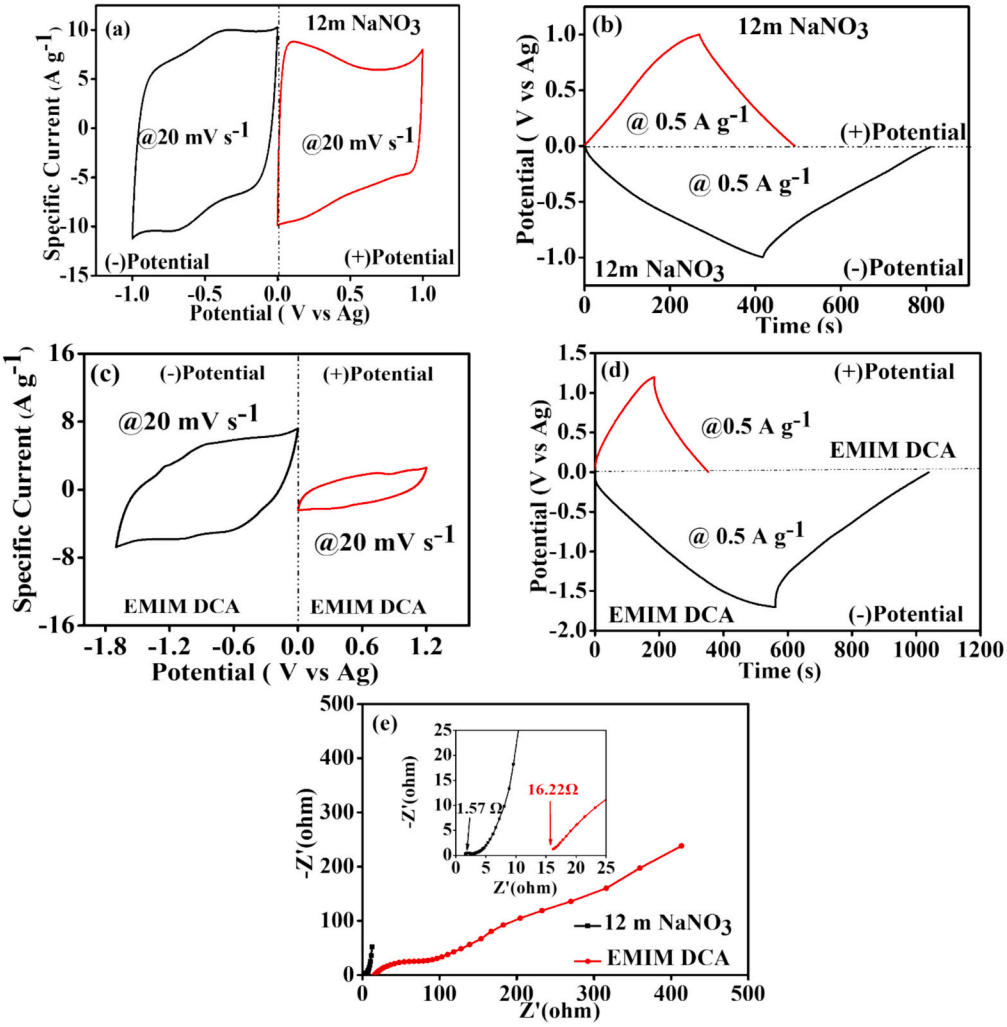

Fig. 3. Electrochemical analysis of N,S-AC electrodes in 12 m $NaNO_3$ and pure EMIM DCA: (a, c) CV at 20 mV s^{-1}, (b, d) GCD at 0.5 A g^{-1}, and (e) EIS Nyquist plots (inset: low-frequency region).

modified solvation structure [23]. The molecular organization within the mixed electrolyte can be understood through a series of cooperative interactions. Sodium ions (Na^+) first coordinate strongly with water molecules, forming compact solvation shells that disrupt extended hydrogen-bonded water clusters. This effect is reinforced by ion pairing between Na^+ and NO_3^-, which further lowers the fraction of unbound water. At the same time, $EMIM^+$ engages in hydrogen bonding with water, competing directly with water–water interactions and thereby weakening the overall hydrogen-bonding network. The dicyanamide anion coordinates simultaneously with both Na^+ and $EMIM^+$, modifying the local electronic environment, a change reflected in the observed shift of the C≡N band. Finally, the participation of NO_3^- in hydrogen bonding with water introduces additional competition for hydration, which destabilizes extended water networks and drives the system toward a more compact and reorganized solvation structure [24]. A detailed compilation of Raman and FTIR spectral data, including peak positions, shifts, and vibrational assignments, is presented in the Supporting information (Tables S1 and S2). These findings demonstrate that the [EMIM DCA]$_1$[$NaNO_3$]$_X$ electrolytes form complex, restructured ionic–molecular networks rather than mere physical blends. The interplay of hydrogen-bonding and electrostatic interactions among the constituent ions fosters enhanced ion mobility, greater stability at the electrode–electrolyte interface, and the ability to operate effectively under high-voltage conditions.

Characterization of the [EMIM DCA]$_1$[$NaNO_3$]$_X$ (x = 1, 2, 3) electrolyte mixtures reveal that variations in the molar ratio of 1-ethyl-3-methylimidazolium dicyanamide (EMIM DCA) to sodium nitrate ($NaNO_3$) significantly alter the solvation environment. These compositional changes modulate the strength and nature of ion-solvent interactions, thereby affecting ionic mobility, the physicochemical properties of water, and the formation of the electric double layer at the electrode-electrolyte interface.

3.2. Electrochemistry measurement

3.2.1. Three-electrode analysis

To rigorously assess the electrochemical performance of binary electrolyte mixtures, the individual electrochemical stability windows (ESWs) of single electrodes in 12 molal (m) sodium nitrate ($NaNO_3$) water-in-salt (WIS) electrolyte and 1-ethyl-3-methylimidazolium dicyanamide (EMIM DCA) were investigated using cyclic voltammetry (CV), galvanostatic charge-discharge (GCD), and electrochemical impedance spectroscopy (EIS). All experiments employed nitrogen and sulfur co-doped activated carbon (N,S-AC) as the working electrode, as detailed in the experimental methodology. Fig. 3(a) and (c) presents the CV profiles of 12 m $NaNO_3$ and EMIM DCA, respectively, recorded at a scan rate of 20 mV s^{-1}. The CV curve for 12 m $NaNO_3$ (Fig. 3(a)) exhibits a near-rectangular shape, spanning a potential window from +1.0 V (positive ESW) to −1.0 V (negative ESW) versus Ag/Ag^+. Within the negative potential region, distinct redox humps are observed in both

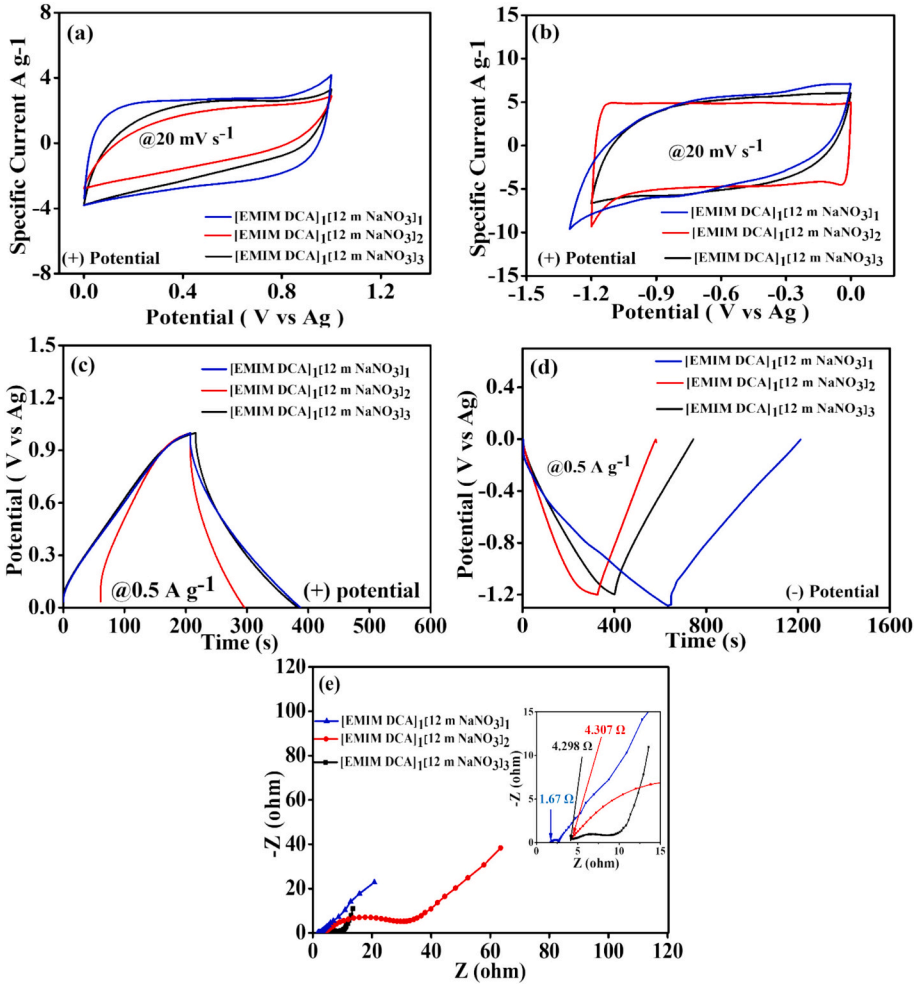

Fig. 4. Electrochemical characterization of N,S-AC electrodes in $[EMIM\ DCA]_1[12\ m\ NaNO_3]_X$ (x = 1, 2, 3): (a, b) CV at 20 mV s^{-1} in positive and negative windows, (c, d) GCD at 0.5 A g^{-1}, and (e) EIS Nyquist plots.

anodic and cathodic sweeps, indicative of pseudocapacitive contributions arising from nitrogen and sulfur heteroatoms integrated into the N, S-AC structure. These redox features are significantly attenuated or absent in the negative potential region, suggesting that interactions between N/S heteroatoms and Na^+ ions predominantly favor electric double-layer capacitance (EDLC) rather than pronounced pseudocapacitive behavior. The substantial current response in 12 m $NaNO_3$ underscores the high charge storage capacity of the N,S-AC electrode. In contrast, the CV curve for EMIM DCA (Fig. 3(c)) displays a distorted profile, deviating from the ideal rectangular shape in both positive and negative potential regions. This deviation is attributed to increased internal resistance and less efficient capacitive performance, likely due to the higher viscosity and larger ionic radii of the $EMIM^+$ cation and DCA^- anion, which impede ion transport. Nevertheless, EMIM DCA demonstrates a broader ESW, extending to −1.6 V in the negative potential region and + 1.0 V in the positive region versus Ag/Ag^+. The GCD profiles of 12 m $NaNO_3$ at a specific current of 0.5 A g^{-1}, shown in Fig. 3 (b), exhibit a quasi-symmetric, linear triangular shape, characteristic of pseudocapacitive behavior. A minimal voltage drop at the onset of the discharge cycle indicates low internal resistance and efficient charge transfer at the electrode–electrolyte interface. In the negative potential region, the N,S-AC electrode achieves a maximum specific capacitance of approximately 207 F g^{-1}. This elevated capacitance is attributed to the synergistic effects of the extended ESW enabled by the concentrated 12 m $NaNO_3$ WIS electrolyte and faradaic contributions from nitrogen and sulfur functional groups on the carbon surface. These active sites likely engage in reversible surface redox reactions with protons (H^+) from the aqueous $NaNO_3$ solution, enhancing overall charge storage capacity. [25]. In the positive potential region, the specific capacitance of the nitrogen- and sulfur-doped activated carbon (N,S-AC) electrode in 12 molal (m) sodium nitrate ($NaNO_3$) water-in-salt (WIS) electrolyte was determined to be approximately 112 F g^{-1}. The galvanostatic charge-discharge (GCD) profiles for 1-ethyl-3-methylimidazolium dicyanamide (EMIM DCA), shown in Fig. 3(d), exhibit a moderately quasi-linear triangular shape with a pronounced internal resistance (IR) drop. This IR drop is primarily attributed to the elevated viscosity and reduced ionic conductivity of EMIM DCA, which hinder efficient ion transport within the electrolyte. Specific capacitance values for EMIM DCA were calculated as 143 F g^{-1} in the negative potential region and 84 F g^{-1} in the positive potential region. These values reflect the distinct interactions between EMIM DCA and the N,S-AC electrode, influenced by the ionic liquid's physicochemical properties. Fig. 3(e) presents a comparative analysis of Nyquist plots derived from electrochemical impedance spectroscopy (EIS) for 12 m $NaNO_3$ and EMIM DCA electrolytes. The 12 m $NaNO_3$ electrolyte demonstrates an equivalent series resistance (ESR) of approximately 1.57 Ω, as illustrated in the inset of Fig. 3(e), consistent with its high ionic conductivity and efficient charge transport within the water-in-salt electrolyte (WiSE) framework. The corresponding Nyquist plot exhibits a small semicircle in the high-frequency region, indicative of a low charge transfer resistance (Rct ≈ 1.24 Ω) and efficient interfacial ion exchange at the electrode–electrolyte interface. At lower frequencies, the nearly vertical

trajectory reflects dominant capacitive behavior with minimal diffusion impedance, suggesting unhindered ion migration through the porous electrode structure. In comparison, the pure EMIM DCA electrolyte shows a significantly higher ESR of 16.22 Ω and an Rct of 50.62 Ω, reflecting limited ionic mobility and elevated internal resistance. The enlarged semicircle at high frequencies indicates slower charge transfer kinetics, while the less vertical slope in the low-frequency region points to restricted ion diffusion and pronounced polarization effects. These phenomena are attributed to the intrinsically higher viscosity and larger ionic radius of $EMIM^+$ and DCA^-, which collectively impede efficient mass transport and slow interfacial charge equilibration [26]. This impedance analysis clearly demonstrates the critical role of electrolyte composition in governing interfacial dynamics and overall electrochemical performance. The WiSE system promotes rapid ion migration and low-resistance charge transfer, whereas the pure ionic liquid experiences hindered transport pathways. Such observations emphasize the necessity of optimizing the balance between ion mobility and viscosity, guiding the rational design of hybrid electrolytes to achieve reduced resistance, fast kinetics, and improved electrochemical reversibility in high-performance supercapacitor devices.

The electrochemical stability of the hybrid electrolytes was examined through linear sweep voltammetry (LSV), and the corresponding curves are presented in the Supporting information (Fig. S1). The results reveal a clear dependence of the electrochemical stability window (ESW) on the electrolyte composition. Among the investigated systems, the equimolar mixture [EMIM DCA]$_1$[12 m $NaNO_3$]$_1$ exhibits the widest ESW, extending from approximately −1.5 V to 1.3 V. This broad potential range suggests a synergistic effect between the ionic liquid and the concentrated aqueous phase, which effectively mitigates water decomposition by reducing the activity of free water molecules and stabilizing the interfacial structure. Increasing the $NaNO_3$ fraction (ratios 1:2 and 1:3) results in a gradual narrowing of the ESW and a decrease in current response, indicating stronger ionic association and limited charge mobility [27]. These observations highlight the importance of composition tuning, as the 1:1 system provides an optimal balance between ionic conductivity and electrochemical stability. Overall, these findings confirm that careful control of the EMIM DCA–$NaNO_3$ ratio is essential for achieving enhanced voltage stability and reliable performance in aqueous-based hybrid supercapacitors. The electrochemical properties of the binary electrolytes [EMIM DCA]$_1$ [12 m $NaNO_3$]$_X$ (x = 1, 2, 3) were further examined. Cyclic voltammetry (CV) profiles recorded at 20 mV s^{-1} (Fig. 4(a) and (b)) display nearly rectangular shapes for all mixtures, confirming capacitive charge storage with additional pseudocapacitive contributions from the heteroatoms in the electrode material. A clear difference is observed in the accessible electrochemical stability window (ESW). The equimolar mixture [EMIM DCA]$_1$[$NaNO_3$]$_1$ offers the broadest ESW, extending from −1.3 V in the negative region to +1.0 V in the positive region versus Ag/Ag^+, corresponding to a total window of 2.3 V. In comparison, the [EMIM DCA]$_1$[12 m $NaNO_3$]$_2$ and [EMIM DCA]$_1$[12 m $NaNO_3$]$_3$ systems reach −1.2 V at the negative limit, with the positive limit still extending to +1.0 V, yielding slightly narrower windows of 2.2 V. The wider ESW of the 1:1 system reflects its enhanced suppression of hydrogen evolution, most likely a consequence of reduced free water content and improved ionic coordination. Interestingly, the best electrochemical response does not coincide with the lowest viscosity. The [EMIM DCA]$_1$[12 m $NaNO_3$]$_3$ mixture exhibits the lowest viscosity (3.18 mPa·s) but underperforms compared to the more viscous [EMIM DCA]$_1$[12 m $NaNO_3$]$_1$ electrolyte (8.42 mPa·s). This highlights that viscosity alone is not the governing parameter for performance. Instead, the coordination structure of the ions and the stability of the solvation network play decisive roles. In the 1:1 mixture, Na^+ ions form compact solvation shells with nitrate, $EMIM^+$ interacts through hydrogen bonding, and DCA^- provides additional coordination. This cooperative arrangement creates a highly ordered ionic environment that minimizes free water, stabilizes the electrode–electrolyte interface, and ensures efficient ion accessibility. FTIR and Raman analyses support this, with O—H and C≡N peak shifts indicating reinforced ion–solvent interactions. By contrast, in the 1:2 and 1:3 systems, excess nitrate disrupts this balance, weakens interactions with $EMIM^+$, and encourages partial ionic aggregation. Although this lowers bulk viscosity, it compromises solvation stability and leads to poorer electrochemical performance [28]. Galvanostatic charge–discharge (GCD) measurements (Fig. 4(c) and (d)) further emphasize these trends. The [EMIM DCA]$_1$[12 m $NaNO_3$]$_1$ mixture achieves the highest capacitances, reaching 112 F g^{-1} at the positive electrode (0 to +1.0 V) and 257 F g^{-1} at the negative electrode (−1.3 to 0 V). In contrast, the 1:2 and 1:3 mixtures display lower capacitances in both regions, confirming that the equimolar composition offers the most favorable balance of ionic interactions. The synergistic role of mixed electrolytes arises from the complementary behaviors of Na^+/NO_3^- and $EMIM^+/DCA^-$ ions within the pore network of N,S-AC. In concentrated water in salt electrolyte (12 m $NaNO_3$), the small Na^+ ions with compact hydration shells penetrate narrow micropores and efficiently contribute to double-layer formation, while disrupting extended water–water clusters. Conversely, the bulkier $EMIM^+$ and DCA^- ions are less hydrated and preferentially occupy mesopores and interact with surface functionalities. This coexistence enables a more effective utilization of pores across different scales. The dynamics of adsorption and desorption also vary between the two electrolytes. Na^+/NO_3^- exhibits rapid transport and reversible confinement in small pores, whereas $EMIM^+/DCA^-$ shows slower diffusion due to its larger size but stabilizes the interfacial structure over wider potential ranges. Their combined presence provides a balance between fast ion kinetics and extended voltage stability [29]. Furthermore, the pseudocapacitive activity of N and S heteroatom sites is influenced by the mixed medium. In 12 m $NaNO_3$, the redox response of pyridinic-N and thiophenic-S sites is facilitated by proton/electron exchange. When $EMIM^+/DCA^-$ is introduced, the reduced water activity and modified local polarity alter the electronic environment around these doped centers, improving reaction reversibility and enhancing their contribution within the accessible voltage window. In this way, the mixed electrolyte simultaneously optimizes double-layer storage and strengthens faradaic interactions at heteroatom sites [30]. Electrochemical impedance spectroscopy (EIS), Fig. 4(e) provides further insight. The 1:1 mixture demonstrates the lowest equivalent series resistance (ESR = 1.67 Ω) and charge-transfer resistance (Rct = 1.04 Ω), confirming efficient ion mobility and fast charge-transfer kinetics. In contrast, the 1:2 and 1:3 mixtures exhibit significantly higher ESR values (4.307 Ω and 3.298 Ω) and larger Rct values (25.325 Ω and 5.772 Ω, respectively), reflecting hindered ion transport and interfacial charge transfer. Taken together, these results demonstrate that the superior performance of the [EMIM DCA]$_1$[12 m $NaNO_3$]$_1$ mixture electrolyte from its well-structured ionic coordination, which enhances interfacial stability and minimizes parasitic reactions. Although the 1:3 electrolyte benefits from lower viscosity, its disrupted solvation structure and partial ion aggregation hinder charge transfer, resulting in reduced capacitance and stability. Thus, the equimolar composition provides the most effective synergy between ionic liquid and salt, achieving the widest ESW, the lowest resistances, and the highest capacitance values.

To investigate the electrochemical behavior of a mixed electrolyte system comprising 1-ethyl-3-methylimidazolium dicyanamide (EMIM DCA) and 12 m $NaNO_3$ in a three-electrode configuration, the pivotal role of the electrolyte's ionic interactions was examined, supported by the properties of the nitrogen- and sulfur-doped activated carbon (N,S-AC) electrode. Cyclic voltammetry (CV) analysis revealed a power-law relationship between the current response (i, in mA) and scan rate (ν), described by the equation, highlighting the dominant influence of the EMIM DCA and $NaNO_3$ electrolyte's unique ionic interactions, enhanced by the N,S-AC electrode's surface chemistry [28,29]:

$$i = a \cdot \nu^b \tag{7}$$

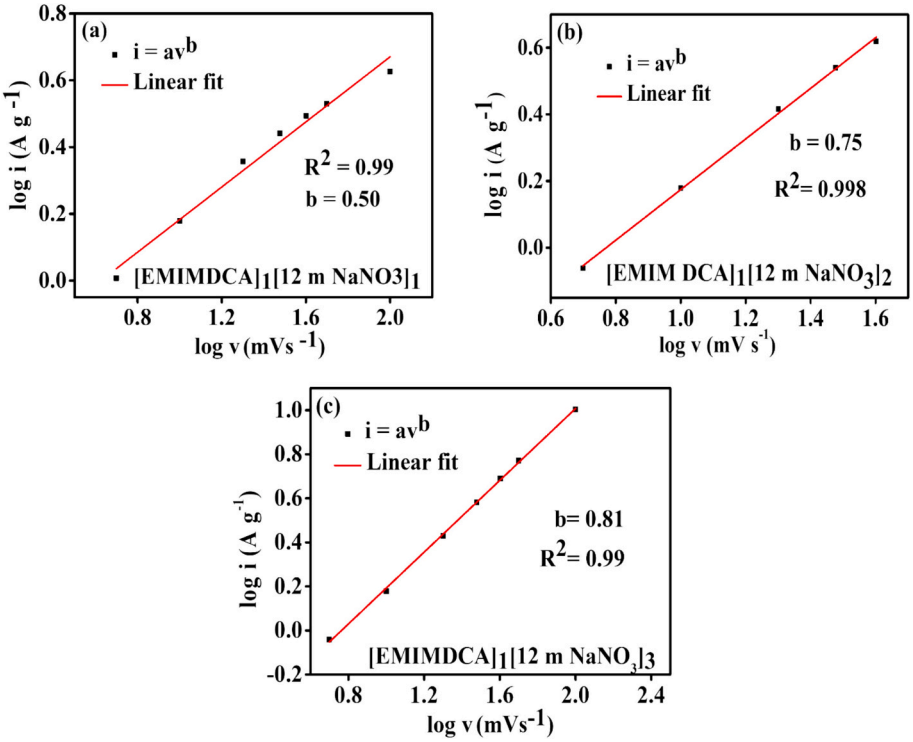

Fig. 5. Logarithmic plots of peak current density versus scan rate for N,S-AC electrodes in binary electrolyte mixtures: (a) [EMIM DCA]$_1$[12 m $NaNO_3$]$_1$, (b) [EMIM DCA]$_1$[12 m $NaNO_3$]$_2$, and (c) [EMIM DCA]$_1$[12 m $NaNO_3$]$_3$.

where (a) and (b) are constants reflecting the electrochemical kinetics and capacitive behavior of the system. The exponent (b) in the power-law relationship (i = a ν^b) serves as a critical parameter for elucidating the electrochemical kinetic behavior of the nitrogen and sulfur co-doped activated carbon (N,S-AC) electrode in the mixed electrolyte. A b value of 0.5 indicates that the current response is predominantly governed by diffusion-limited processes, where the transport of ions or molecules through the electrolyte dictates the reaction kinetics. Conversely, a b value of 1.0 signifies a surface-controlled, capacitive mechanism, characterized by rapid reactions at the electrode surface with minimal dependence on ion diffusion. Intermediate b values between 0.5 and 1.0 reflect a hybrid regime, where both diffusion-controlled and surface capacitive processes contribute to the overall current response [31]. The electrochemical behavior of the [EMIM DCA]$_1$[12 m $NaNO_3$]$_X$ (x = 1, 2, 3) electrolyte system, paired in nitrogen- and sulfur-doped activated carbon (N,S-AC) electrode, was analyzed to assess the influence of this mixed electrolyte on charge storage mechanisms. As shown in Fig. 5(a), the [EMIM DCA]$_1$[12 m $NaNO_3$]$_1$ electrolyte displays a b-value of 0.5 in the power-law relation (i = a ν^b), signifying that the charge storage process is predominantly governed by ion diffusion. This characteristic can be linked to the strong ionic interactions present in the mixed system, which likely hinder ion transport and promote diffusion-limited kinetics. Conversely, the [EMIM DCA]$_1$[12 m $NaNO_3$]$_2$ and [EMIM DCA]$_1$[12 m $NaNO_3$]$_3$ systems, illustrated in Fig. 5(b) and (c), exhibit b-values of 0.75 and 0.81, respectively, reflecting a transition toward a mixed charge storage mechanism that involves both capacitive surface reactions and diffusion-controlled processes. These higher b values reflect the enhanced contribution of capacitive mechanisms, driven by variations in the molar ratio of 1-ethyl-3-methylimidazolium dicyanamide (EMIM DCA) to 12 molal (m) sodium nitrate ($NaNO_3$). The power-law analysis highlights the tunability of the system's electrochemical kinetics through compositional adjustments, with the $NaNO_3$:EMIM DCA ratio significantly influencing charge storage dynamics. To quantify the relative contributions of capacitive and diffusion-controlled processes to the total charge storage, the Dunn method was employed. This approach, based on a modified power-law relationship, deconvolutes the total current (i) at specific potentials, particularly near peak regions in cyclic voltammetry (CV) curves, into two components: A capacitive contribution proportional to the scan rate ($k_1\nu$) and a diffusion-controlled contribution proportional to the square root of the scan rate ($k_2\,\nu^{1/2}$). The governing equation is expressed as:

$$i = k_1\nu + k_2\nu^{1/2} \tag{8}$$

Rearranging this equation yields:

$$\frac{i}{\nu^{1/2}} = k_1\,\nu^{1/2} + k_2 \tag{9}$$

A linear plot of $i/\nu^{1/2}$ versus $\nu^{1/2}$, commonly referred to as a Dunn plot, allows for the extraction of the constants k_1 or k_2 from the slope and intercept, respectively [32]. This method enables precise differentiation of surface and diffusion limited charge storage mechanisms, providing deeper insight into the electrochemical performance of the electrolyte mixtures.

The contributions of surface-controlled and diffusion-controlled capacitance for the nitrogen- and sulfur-doped activated carbon (N,S-AC) electrode in the hybrid electrolyte mixtures [EMIM DCA]$_1$[12 m $NaNO_3$]$_X$ (x = 1, 2, 3) are presented in Fig. 6(a)-(d). At a scan rate of 5 mV s^{-1}, the surface-controlled capacitance contributions were approximately 29 %, 3 %, and 1 % for the [EMIM DCA]$_1$[12 m $NaNO_3$]$_3$, [EMIM DCA]$_1$[12 m $NaNO_3$]$_2$, and [EMIM DCA]$_1$[12 m $NaNO_3$]$_1$ mixture, respectively. These results indicate that the charge storage mechanism is predominantly diffusion-controlled across all electrolyte compositions.

This diffusion-dominated behavior arises from the reversible intercalation and deintercalation of Na^+ ions within the porous, heteroatom-enriched N,S-AC framework. The corresponding electrochemical reactions can be represented as follows:

During Discharge (sodiation/Na + insertion):

$$N,S-AC + xNa^+ + xe^- \rightarrow NaxN,S-AC \tag{10}$$

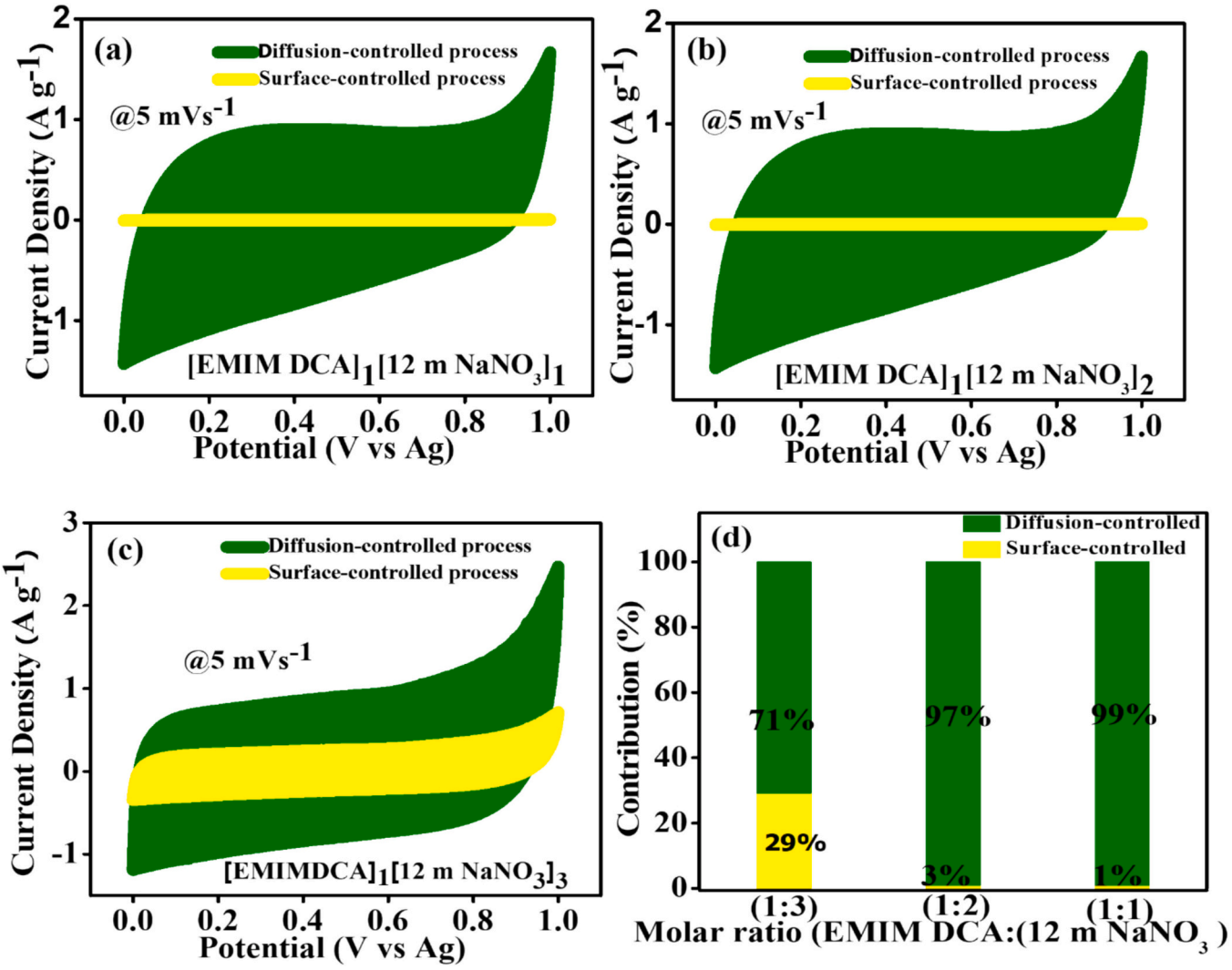

Fig. 6. CV responses of N,S-AC electrodes in $[EMIM\ DCA]_1[12\ m\ NaNO_3]_X$ (x = 1–3), highlighting the dominance of diffusion-controlled charge storage and the distribution of surface- versus diffusion-controlled contributions.

Table 1
Summary of desolvated and solvated ion of the 12 m $NaNO_3$ and EMIM DCA electrolyte.

Electrolyte ions	Bare/desolvated ion (nm)	Solvated ion (nm)
$EMIM^+$	~0.34	~0.60/(−)
DCA^-	~0.26	~0.40/(−)
Na^+	~0.095	~0.36
NO_3^-	~0.179	~0.335

During Charge (Desodiation/Na + extraction):

$$NaxN,S-AC \rightarrow N,S-AC + xNa^+ + xe^- \quad (11)$$

During charging in the $[EMIM\ DCA]_1[12\ m\ NaNO_3]_X$ system, Na^+ ions diffuse into the porous N,S-AC electrode and preferentially occupy defect-rich or heteroatom-doped sites, enhancing electrochemical activity. This ion intercalation is coupled with electron transfer through the external circuit, maintaining charge neutrality and enabling efficient charge storage within the electrode's porous architecture [31]. The larger 1-ethyl-3-methylimidazolium ($EMIM^+$) cations are sterically hindered from entering the N,S-AC lattice. Instead, $EMIM^+$ ions adsorb onto the electrode surface, contributing primarily to electric double layer (EDL) formation rather than intercalation processes. During discharge, the previously intercalated Na^+ ions are released back into the electrolyte, accompanied by electron flow in the external circuit, generating the discharge current. These reversible ion dynamics occur without significant structural degradation of the electrode, ensuring stable cycling performance and long-term durability. The enhanced diffusion-controlled charge storage observed in the $[EMIM\ DCA]_1[12\ m\ NaNO_3]_1$ mixture is closely related to the prevalence of desolvated ions, as summarized in Table 1. Incorporation of nitrogen and sulfur heteroatoms into the NS-A,C framework introduces polar functional groups, such as pyridinic-N and thiophenic-S, which modify the surface chemistry and electronic structure of the carbon material. These dopant-induced functionalities enhance surface polarity and electron distribution, facilitating stronger Na^+ adsorption and promoting efficient intercalation. Consequently, the N,S-SAC electrode in the $[EMIM\ DCA]_1[12\ m\ NaNO_3]_1$ electrolyte demonstrates enhanced ion–electrode interactions, supporting predominantly diffusion-controlled charge storage and positioning it as a promising candidate for high-performance supercapacitor applications [8,33].

The superior electrochemical performance of the $[EMIM\ DCA]_1[12\ m\ NaNO_3]_1$ electrolyte mixture, when paired with nitrogen and sulfur co-doped activated carbon (N,S-AC) electrodes, is primarily driven by the prevalence of desolvated ions, as confirmed by Fourier-transform infrared (FTIR) spectroscopy. The FTIR analysis reveals a significant reduction in free water molecules available for ion solvation in the 1:1

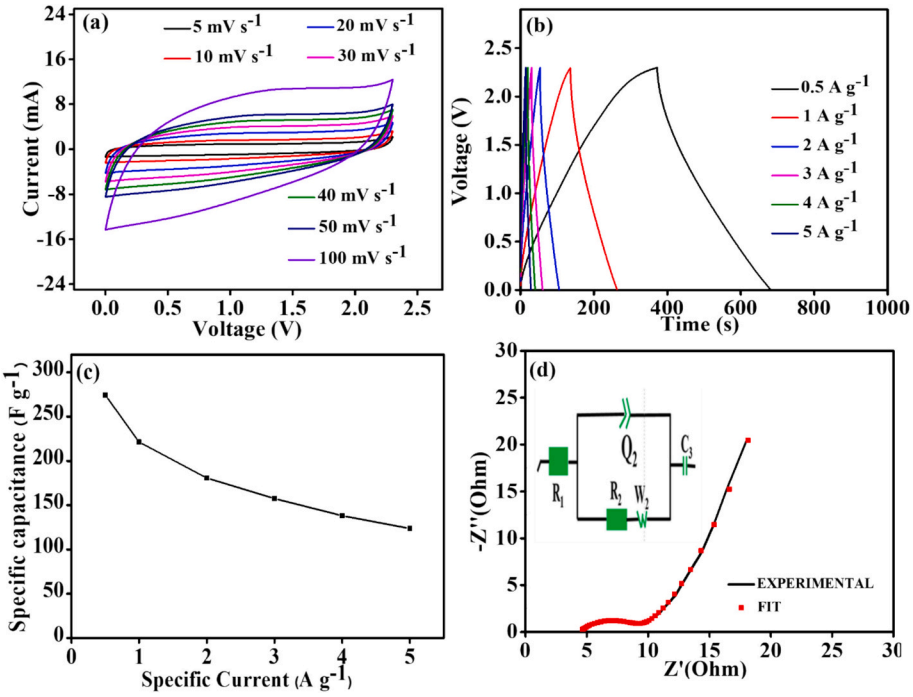

Fig. 7. Electrochemical characterization of a symmetric supercapacitor (N,S-AC//N,S-AC) in [EMIM DCA]$_1$[12 m $NaNO_3$]$_1$ electrolyte: (a) (CV) profiles at various scan rates, (b) (GCD) curves at different specific currents, (c) specific capacitance as a function of specific current, and (d) Nyquist plot with an inset showing the equivalent circuit model used for data fitting.

molar ratio, resulting in an optimized water-to-salt balance. This condition promotes a higher concentration of unsolvated Na^+ ions, which can more effectively intercalate into the porous N,S-AC matrix, thereby enhancing specific capacitance and broadening the electrochemical stability window (ESW). In contrast, increasing the $NaNO_3$ proportion in the [EMIM DCA]$_1$[12 m $NaNO_3$]$_2$ and [EMIM DCA]$_1$[12 m $NaNO_3$]$_3$ mixtures elevates the water content, leading to greater ion solvation. This increased solvation results in a higher population of hydrated ions with larger ionic radii, which impede intercalation into the carbon matrix and shift the charge storage mechanism toward surface-controlled (capacitive) behavior. These trends are substantiated by power-law analysis (Fig. 5), which highlights the influence of molar ratio on charge storage kinetics and further corroborated by the Dunn method (Fig. 6), which quantifies the relative contributions of diffusion-controlled and surface-controlled processes.

3.2.2. *Two-electrode (full-cell) analysis*

To evaluate the performance of the binary electrolyte system, a symmetric supercapacitor (SC) was fabricated using nitrogen and sulfur co-doped activated carbon (N,S-AC) electrodes, selected for their superior electrochemical properties. Despite using the same electrode material on both sides, differing operating voltage windows and specific capacitances were observed: the negative electrode exhibited a potential window of −1.3 V with a capacitance of 257 F g^{-1}, while the positive electrode operated at 1.0 V with a capacitance of 112 F g^{-1}. To ensure charge balance within the device, electrode masses were adjusted according to these parameters using the mass balance equation (Eq. (6)). For a total active material mass of 4.7 mg, the calculated electrode masses were approximately 1.18 mg for the negative electrode and 3.52 mg for the positive electrode. This mass balancing approach was critical to optimize the electrochemical performance and energy storage efficiency of the device. The electrolyte consisted of a 1:1 molar ratio mixture of 1-ethyl-3-methylimidazolium dicyanamide (EMIM DCA) and 12 m $NaNO_3$, denoted as [EMIM DCA]$_1$[12 m $NaNO_3$]$_1$. Cyclic voltammetry (CV) profiles of the SC employing the [EMIM DCA]$_1$[12 m $NaNO_3$]$_1$ electrolyte were evaluated across a range of scan rates (5, 10, 20, 30, 40, 50, and 100 mV s^{-1}) at an operating voltage of 2.3 V, as shown in Fig. 7(a). At lower scan rates (5–50 mV s^{-1}), the CV curves exhibit a near-ideal rectangular shape, indicative of efficient ion transport and characteristic of pseudocapacitive behavior. However, at higher scan rates beyond 50 mV s^{-1}, deviations from the rectangular profile become evident, suggesting limitations in ion diffusion under rapid scan rate conditions [34]. The observed deviations in the cyclic voltammetry (CV) profiles of the symmetric supercapacitor at higher scan rates are likely due to the predominance of micropores within the nitrogen- and sulfur-co-doped activated carbon (N,S-AC) electrodes. These micropores restrict the efficient infiltration of the relatively large dicyanamide (DCA^-) anions from the [EMIM DCA]$_1$[12 m $NaNO_3$]$_1$ electrolyte, limiting ion diffusion and impacting charge storage performance under high-rate conditions [35]. The restricted accessibility of the relatively large dicyanamide (DCA^-) anions to the microporous structure of the nitrogen- and sulfur-co-doped activated carbon (N,S-AC) electrodes in the [EMIM DCA]$_1$[12 m $NaNO_3$]$_1$ electrolyte system limits efficient ion infiltration, particularly under rapid electrochemical cycling conditions. This constraint hampers the formation of the electric double layer, resulting in reduced capacitance due to diminished ion accessibility to the internal pore surfaces of the electrode. Fig. 7(b) presents the galvanostatic charge–discharge (GCD) profiles of the symmetric supercapacitor using the [EMIM DCA]$_1$[12 m $NaNO_3$]$_1$ electrolyte at current densities of 0.5, 1, 2, 3, 4, and 5 A g^{-1}. The nearly symmetric triangular shapes of the GCD curves are consistent with the pseudocapacitive behavior observed in the cyclic voltammetry (CV) profiles shown in Fig. 7(a). Specific capacitance values (C_s), derived from the GCD data using Eq. (2), are plotted against current density in Fig. 7(c). In this symmetric device, the nitrogen and sulfur co-doped activated carbon (N,S-AC) electrodes paired with the optimized electrolyte exhibited a notable single-electrode specific capacitance of 273.41 F g^{-1} at 0.5 A g^{-1}. This performance reflects the combined effect of the heteroatom-enriched porous carbon framework and the carefully engineered ionic environment of the hybrid electrolyte, which together facilitate efficient ion transport and surface redox reactions. As the current density increased, a decline in capacitance was observed, which

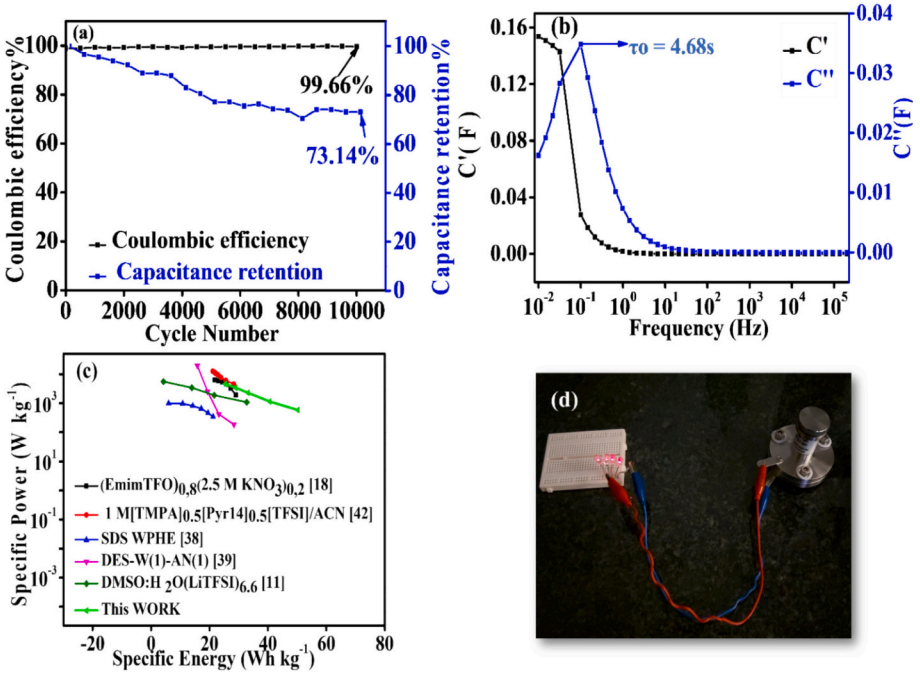

Fig. 8. Electrochemical performance of the [EMIM DCA]$_1$[12 m $NaNO_3$]$_1$ electrolyte in a symmetric N,S-AC//N,S-AC supercapacitor: (a) cycling stability and coulombic efficiency, (b) real and imaginary capacitance vs. frequency, (c) Ragone plot comparing energy and power densities, and (d) photograph of the device powering four LEDs.

is commonly attributed to limited ion diffusion and reduced time for ion adsorption at higher rates. Despite this decrease, the electrode maintained a capacitance of 123.76 F g^{-1} at 5 A g^{-1}, retaining approximately 45.3 % of its initial capacitance. Such retention demonstrates strong rate capability and suggests effective interfacial compatibility and ion mobility within the electrode–electrolyte system. Notably, the specific capacitance tends to stabilize at higher current densities, indicating that the device can sustain robust performance even under rapid cycling conditions. These findings underscore the potential of combining functionalized carbon materials with mixed ionic liquid–water-in-salt electrolytes to develop supercapacitors that are both durable and capable of delivering high energy densities [36]. Electrochemical impedance spectroscopy (EIS) results, shown in Fig. 7(d), display experimental and fitted Nyquist plots for the supercapacitor. The low-frequency region exhibits a near-vertical line along the negative imaginary axis (−Z″), characteristic of capacitive behavior. The EIS data were analyzed using the Z Fit module in EC-Lab® software (version 11.50), employing an equivalent circuit model comprising R_1 (solution resistance), R_2 (charge transfer resistance), Q_2 (constant phase element modelling non-ideal double-layer capacitance), W_2 (Warburg element representing ion diffusion), and C_3 (combined real and mass capacitance). The fitted resistance values were 4.37 Ω for R_1 and 5.19 Ω for R_2, closely aligning with the experimental values of 4.68 Ω and 5.26 Ω, respectively, validating the accuracy of the proposed model. These resistance values account for contributions from the ionic resistance of the electrolyte, the intrinsic resistance of the N,S-AC electrode, and contact resistances at the electrode/current collector and electrode/electrolyte interfaces.

The long-term cycling stability of the N,S-AC//N,S-AC symmetric device operating in the [EMIM DCA]$_1$[12 m $NaNO_3$]$_1$ electrolyte is presented in Fig. 8(a). The capacitance evolution initially rises due to progressive activation of the N,S-co-doped carbon surface, where improved electrolyte infiltration and ion accessibility enhance charge accumulation. The heteroatom functionalities (N and S) provide additional redox-active sites that become increasingly accessible during cycling, contributing to pseudocapacitive enhancement. A gradual decline in capacitance, observed between approximately 3000 to 4000 cycles, is attributed to minor structural rearrangements of the electrode and the formation of a thin solid electrolyte interface (SEI) as layer that stabilizes the electrode–electrolyte interface. Partial aggregation of EMIM DCA species may further limit ionic mobility, a transient behavior typical of hybrid ionic liquid–salt systems. However, the well-organized solvation network within the [EMIM DCA]$_1$[12 m $NaNO_3$]$_1$ electrolyte where Na^+ forms compact coordination shells, NO_3^- interacts strongly with Na^+, and $EMIM^+$ engages in hydrogen bonding promotes stable ion transport and suppresses parasitic reactions, as evidenced by FTIR and Raman analyses. After the initial adjustment period, the capacitance becomes stable, reflecting the durable molecular organization of the electrolyte that supports sustained performance. This stabilization, observed after roughly 4000 cycles, suggests that the structured solvation environment efficiently maintains interfacial integrity and minimizes degradation over prolonged cycling. The device retains about 83.33 % of its initial capacitance after 10,000 cycles with a high coulombic efficiency of 99.66 %,indicating reversible charge storage and excellent interfacial compatibility between the N,S-AC electrode and the mixture electrolyte [37]. To gain deeper insight into the rate-dependent behavior of the device, galvanostatic cycling was conducted across a broad range of current densities (1–10 A g^{-1}), as presented in the Supporting information (Fig. S2). At a low current density of 1 A g^{-1}, the device exhibits a gradual decrease in capacitance, characteristic of diffusion-limited charge storage. In this regime, Na^+ ions penetrate deeper into the microporous structure of the N,S-AC electrode, encountering higher ionic resistance and slower transport pathways, which result in partial ion confinement. This observation aligns with the power-law fitting ($b \approx 0.5$), confirming that the dominant contribution to charge storage arises from diffusion-controlled intercalation processes rather than purely surface adsorption. At elevated current densities (≥5 A g^{-1}), the device maintains over 90 % of its initial capacitance, demonstrating remarkable rate stability. This behavior highlights the synergistic effect between the porous carbon framework and the well-organized solvation network of the [EMIM DCA]$_1$[$NaNO_3$]$_1$ electrolyte. Within this hybrid medium, compact Na^+ coordination and strong Na^+–NO_3^- associations facilitate rapid ion transport, while hydrogen bonding between $EMIM^+$ cations and surrounding species stabilizes the interfacial environment. These cooperative interactions

Table 2
Mixture electrolyte-aqueous electrolyte carbon-based symmetric devices performances comparison.

Material	Electrolyte	Cs_{ingle} (F g^{-1})	Cell voltage (V)	E_S (Wh kg^{-1})	P_{max} (W kg^{-1})	Ref
AC//AC	SDS WPHE	120	2.3	18	43	[38]
AC//AC	DES-W (1)-AN (1)	186.4	2.2	28.6	–	[39]
AC//AC	LiTFSI $(H_2O)_{2.6}(CH_3CN)_{3.7}$	108	2.2	–	–	[13]
AC//AC	HE-$NaClO_4$	154.8	2.71	39.2	–	[40]
AC//AC	Propionitrile (PN) + AN	94.8	2.7	25.1	6870	[34]
AC//AC	3 m $NaClO_4$-25 %H_2O-75 % PEGDME	112.8	2.4	22.6	12,000	[41]
AC//AC	1 M$[TMPA]_{0.5}[Pyr14]_{0.5}$[TFSI]/ACN	100	3.1	28.30	26,950	[42]
AC//AC	$[EmimTFO]_{0.8}[2.5MKNO_3]_{0.2}$	138.6	2.1	24.5	4000	[18]
RGO//RGO	2 M $EMIMBF_4$/AN	158.3	3.4	62.6	16,400	[6]
AC//AC	17 m $NaClO_4$	236	2.4	28.1	5109	[41]
AC//AC	1.0MLiTFSI(aq.)/MPPyrroTFSI	131	2.2	22	–	[15]
N,S-AC//N,S-AC	12 m $NaNO_3$	180	2	25	10,000	[8]
N,S-AC//N,S-AC	$[12mNaNO_3]_1$[EMIM DCA]$_1$	273.41	2.3	50.22	4599	This work

effectively suppress concentration polarization and structural fatigue, allowing the electrode to retain high reversibility even under accelerated charge–discharge conditions. Fig. 8(b) depicts the real (C′) and imaginary (C″) components of capacitance as functions of frequency, revealing a relaxation time of less than 4.68 s for the symmetric SC. This rapid relaxation time indicates the device's capability for fast charge–discharge processes, enhancing its suitability for high-rate applications. The electrochemical performance of the assembled symmetric supercapacitor was evaluated in terms of energy and power densities, as illustrated in the Ragone plot (Fig. 8(c)). At a current density of 0.5 A g^{-1}, the device delivered a specific energy of 50.22 W h kg^{-1} with a corresponding specific power of 583.97 W kg^{-1}, indicating efficient energy storage at moderate operating conditions. When tested at a higher current density of 5 A g^{-1}, the specific energy decreased to 22.73 W h kg^{-1}, reflecting the expected inverse relationship between energy and power under fast charge–discharge cycles. Notably, even at this elevated current, the device achieved a maximum specific power of 4599 W kg^{-1}, highlighting its excellent ability to deliver energy rapidly. Table 2 includes key metrics such as specific energy (E_S), specific power (P_S), operating voltage, and capacitance, allowing a clear evaluation of the advantages offered by the [EMIM DCA]$_1$[12 m $NaNO_3$]$_1$-based system. The results demonstrate that the current device not only competes with but in many cases outperforms other reported systems, particularly in terms of energy–power balance. Fig. 8(d) presents a photograph of the device powering four light-emitting diodes (LEDs). The device sustained illumination for approximately 64 s, highlighting its practical utility and potential for real-world energy storage applications. This reinforces the practical applicability of the proposed electrolyte–electrode combination in high-performance energy storage technologies.

4. Conclusion

This study introduces a cost-effective and scalable electrolyte engineering strategy aimed at enhancing the electrochemical performance of supercapacitors. By incorporating 1-ethyl-3-methylimidazolium dicyanamide (EMIM DCA) into a highly concentrated aqueous solution of sodium nitrate (12 m $NaNO_3$), a hybrid electrolyte system was developed that effectively balances ionic conductivity, stability, and electrochemical activity. The integration of EMIM DCA significantly broadened the electrochemical stability window by suppressing water activity and mitigating parasitic reactions at the electrode interface key limitations in conventional aqueous electrolytes. Electrochemical evaluation of nitrogen- and sulfur-co-doped activated carbon (N,S-AC) electrodes in this electrolyte revealed a high specific capacitance of 257 F g^{-1} in a three-electrode setup, demonstrating the synergistic effect of electrolyte–electrode compatibility. When implemented in a symmetric device (N,S-AC//N,S-AC) with a 1:1 molar ratio of [EMIM DCA]$_1$[12 m $NaNO_3$]$_1$, the system delivered an extended operating voltage of 2.3 V. This enabled a specific energy of 50.22 W h kg^{-1} and a maximum specific power of 4555 W kg^{-1} at 5 A g^{-1}, positioning the device among the top performers in its class, as highlighted in the Ragone plot (Fig. 8c) and benchmarked in Table 2 against literature-reported systems. Beyond energy and power metrics, the device exhibited outstanding durability, retaining 83.33 % of its original capacitance over 10,000 charge–discharge cycles, confirming the long-term operational stability of the hybrid system. These findings underscore the practical promise of ionic liquid/water-in-salt mixtures as next-generation electrolytes for high-voltage, high-performance supercapacitors. The optimized [EMIM DCA]$_1$[12 m $NaNO_3$]$_1$ formulation offers a compelling route toward environmentally benign, high-efficiency energy storage devices suited for renewable energy integration, electric mobility, and other emerging applications demanding both power and longevity.

CRediT authorship contribution statement

S. Thior: Writing – original draft, Investigation, Formal analysis, Data curation, Conceptualization. **V.N. Kitenge:** Writing – review & editing, Formal analysis, Data curation, Conceptualization. **Ndeye F. Diop:** Writing – review & editing, Formal analysis, Data curation, Conceptualization. **Kabir O. Otun:** Writing – review & editing, Formal analysis, Data curation. **V.M. Maphiri:** Writing – review & editing, Formal analysis. **Rashed A.M. Adam:** Formal analysis, Writing – review & editing. **Balla D. Ngom:** Writing – review & editing, Supervision, Project administration, Methodology, Conceptualization. **N. Manyala:** Writing – review & editing, Supervision, Resources, Project administration, Methodology, Funding acquisition, Conceptualization.

Declaration of competing interest

The authors declare that they have no known competing financial interests or personal relationships that could have appeared to influence the work reported in this paper.

Acknowledgment

Financial support was provided by the National Research Foundation (NRF) South African Research Chairs Initiative (SARChI) and the University of Pretoria co-funded chair (Grant RNEWSW240307208354). The opinions, findings, conclusions, and recommendations expressed in this publication are those of the author(s) and do not necessarily reflect the views of the NRF or the University of Pretoria, neither of which accepts liability in this regard.

Appendix A. Supplementary data

Supplementary data to this article can be found online at https://doi.org/10.1016/j.est.2025.119425.

Data availability

Data will be made available on request.

References

[1] B. Li, F. Dai, Q. Xiao, L. Yang, J. Shen, C. Zhang, M. Cai, Nitrogen-doped activated carbon for a high energy hybrid supercapacitor, Energy Environ. Sci. 9 (2016) 102–106, https://doi.org/10.1039/c5ee03149d.

[2] N. Kumar, R. Aepuru, S.Y. Lee, S.J. Park, Recent advances in phosphorene: a promising material for supercapacitor applications, Mater. Sci. Eng. R. Rep. 163 (2025), https://doi.org/10.1016/j.mser.2025.100932.

[3] L. Timperman, A. Vigeant, M. Anouti, Eutectic mixture of protic ionic liquids as an electrolyte for activated carbon-based supercapacitors, Electrochim. Acta 155 (2015) 164–173, https://doi.org/10.1016/j.electacta.2014.12.130.

[4] L. Pradhan, T.K. Das, B.K. Jena, Advances in next-generation electrochromic supercapacitors: emerging applications, challenges and future perspectives, Sustain. Energy Fuels (2025), https://doi.org/10.1039/D4SE01551G.

[5] H. Pan, X. Jiao, W. Zhang, L. Fan, Z. Yuan, C. Zhang, Supercapacitor with ultra-high power and energy density enabled by nitrogen/oxygen-doped interconnected hollow carbon nano-onions, Chem. Eng. J. 484 (2024), https://doi.org/10.1016/j.cej.2024.149663.

[6] S.I. Wong, H. Lin, J. Sunarso, B.T. Wong, B. Jia, Optimization of ionic-liquid based electrolyte concentration for high-energy density graphene supercapacitors, Appl. Mater. Today 18 (2020), https://doi.org/10.1016/j.apmt.2019.100522.

[7] D. Xiao, L. Zhang, Z. Li, H. Dou, X. Zhang, Design strategies and research progress for water-in-salt electrolytes, Energy Storage Mater. 44 (2022) 10–28, https://doi.org/10.1016/j.ensm.2021.09.035.

[8] S. Thior, V.N. Kitenge, K.O. Otun, R.A.M. Adam, N.F. Diop, B.D. Ngom, N. Manyala, Influence of water-in-salt electrolytes on the electrochemical performance of porous N and S co-doped carbon electrodes in supercapacitors, New J. Chem. (2024), https://doi.org/10.1039/d4nj04507f.

[9] M. Pang, S. Jiang, J. Zhao, S. Zhang, R. Wang, N. Li, R. Liu, Q. Pan, W. Qu, B. Xing, "Water-in-salt" electrolyte enhanced high voltage aqueous supercapacitor with carbon electrodes derived from biomass waste-ground grain hulls, RSC Adv. 10 (2020) 35545–35556, https://doi.org/10.1039/d0ra07448a.

[10] L. Suo, O. Borodin, T. Gao, M. Olguin, J. Ho, X. Fan, C. Luo, C. Wang, K. Xu, "Water-in-salt" electrolyte enables high-voltage aqueous lithium-ion chemistries, n.d. https://www.science.org.

[11] X. Lu, R.J. Jiménez-Riobóo, D. Leech, M.C. Gutiérrez, M.L. Ferrer, F. Del Monte, Aqueous-eutectic-in-salt electrolytes for high-energy-density supercapacitors with an operational temperature window of 100 °C, from-35 to +65 °C, ACS Appl. Mater. Interfaces 12 (2020) 29181–29193, https://doi.org/10.1021/acsami.0c04011.

[12] Q. Dou, Y. Lu, L. Su, X. Zhang, S. Lei, X. Bu, L. Liu, D. Xiao, J. Chen, S. Shi, X. Yan, A sodium perchlorate-based hybrid electrolyte with high salt-to-water molar ratio for safe 2.5 V carbon-based supercapacitor, Energy Storage Mater. 23 (2019) 603–609, https://doi.org/10.1016/j.ensm.2019.03.016.

[13] Q. Dou, S. Lei, D.W. Wang, Q. Zhang, D. Xiao, H. Guo, A. Wang, H. Yang, Y. Li, S. Shi, X. Yan, Safe and high-rate supercapacitors based on an "acetonitrile/water in salt" hybrid electrolyte, Energy Environ. Sci. 11 (2018) 3212–3219, https://doi.org/10.1039/c8ee01040d.

[14] Q. Dou, Y. Wang, A. Wang, M. Ye, R. Hou, Y. Lu, L. Su, S. Shi, H. Zhang, X. Yan, "Water in salt/ionic liquid" electrolyte for 2.8 V aqueous lithium-ion capacitor, Sci. Bull. (Beijing) 65 (2020) 1812–1822, https://doi.org/10.1016/j.scib.2020.07.009.

[15] S. Sathyamoorthi, M. Sawangphruk, A simple and practical hybrid ionic liquid/aqueous dual electrolyte configuration for safe and ion-exchange membrane-free high cell potential supercapacitor, Electrochim. Acta 305 (2019) 443–451, https://doi.org/10.1016/j.electacta.2019.03.090.

[16] V.N. Kitenge, D.J. Tarimo, G. Rutavi, V.M. Maphiri, S. Sarr, M. Diop, M. Chaker, N. Manyala, Influence of nitrogen and sulfur co-doped activated carbon used as electrode material in EmiFSI ionic liquid toward high-energy supercapacitors, J. Energy Storage 81 (2024), https://doi.org/10.1016/j.est.2024.110453.

[17] Y. Zhou, P. Jin, Y. Zhou, Y. Zhu, High-performance symmetric supercapacitors based on carbon nanotube/graphite nanofiber nanocomposites, Sci. Rep. 8 (2018), https://doi.org/10.1038/s41598-018-27460-8.

[18] V.N. Kitenge, D.J. Tarimo, K.O. Oyedotun, G. Rutavi, D.T. Bakhoum, N. Manyala, Electrical double-layer capacitor based on low aqueous electrolyte contents in EmimTFO ionic liquid, Int. J. Energy Res. 2023 (2023), https://doi.org/10.1155/2023/8659009.

[19] The Mass-Balancing between Positive and Negative Electrodes for Optimizing Energy Density of Supercapacitors, (n.d.).

[20] N. Kamboj, R.S. Dey, Exploring the chemistry of "organic/water-in-salt" electrolyte in graphene-polypyrrole based high-voltage (2.4V) microsupercapacitor, Electrochim. Acta 421 (2022), https://doi.org/10.1016/j.electacta.2022.140499.

[21] R. Pamies, M.D. Avilés, J. Arias-Pardilla, F.J. Carrión, J. Sanes, M.D. Bermúdez, Rheological study of new dispersions of carbon nanotubes in the ionic liquid 1-ethyl-3-methylimidazolium dicyanamide, J. Mol. Liq. 278 (2019) 368–375, https://doi.org/10.1016/j.molliq.2019.01.074.

[22] Z. Zhang, J. Feng, Y. Jiang, J. Feng, High-pressure salt templating strategy toward intact isochoric hierarchically porous carbon monoliths from ionic liquids, RSC Adv. 7 (2017) 51096–51103, https://doi.org/10.1039/c7ra09823e.

[23] S. Konwar, S. Kumar, A.A. Mohamad, A. Jain, M. Michalska, V.D. Punetha, M.Z. A. Yahya, K. Strzałkowski, D. Singh, M. Diantoro, F.I. Chowdhury, P.K. Singh, Ionic liquid (1-ethyl-3-methylimidazolium tricyanomethanide) incorporated corn starch polymer electrolyte for solar cell and supercapacitor application, Chem. Phys. Impact 10 (2025) 100780, https://doi.org/10.1016/j.chphi.2024.100780.

[24] M. Karnan, K. Hari Prakash, S. Badhulika, Revealing the super capacitive performance of N-doped hierarchical porous activated carbon in aqueous, ionic liquid, and redox additive electrolytes, J. Energy Storage 53 (2022), https://doi.org/10.1016/j.est.2022.105189.

[25] A. Azizpour, N. Bagovic, N. Ploumis, K. Mylonas, D. Hoxha, F. Kienberger, N. Al-Zubaidi-R-Smith, G. Gramse, Electrochemical analysis of carbon-based supercapacitors using finite element modeling and impedance spectroscopy, Energies (Basel) 18 (2025), https://doi.org/10.3390/en18061450.

[26] H. Wang, W. Liu, J. Huang, T. Xiao, W. Lei, F. Gao, M. Liu, High output voltage aqueous supercapacitors by water deactivated electrolyte over wide temperature range, Adv. Sci. (2025), https://doi.org/10.1002/advs.202500385.

[27] A. Husain, M. Kandasamy, D.K. Mahajan, M. Selvaraj, R. Ahmad, M.A. Assiri, N. Kumar, V.K. Ramachandaramurthy, Attaining promising efficiency through a quasi-solid-state symmetrical supercapacitor and dye-sensitized solar cell counter electrode utilizing bifunctional nitrogen-doped microporous activated carbon, Inorg. Chem. Commun. 168 (2024), https://doi.org/10.1016/j.inoche.2024.112859.

[28] S. Pany, A. Nashim, R. Mohanty, K. Parida, Deciphering the electrochemical kinetics of sulfur vacancy-assisted nitrogen-doped NiCo2S4 combined with sulfur-doped g-C3N4 towards supercapacitor applications, Mater. Adv. (2025), https://doi.org/10.1039/d4ma00847b.

[29] Y. Chang, H. Shi, X. Yan, G. Zhang, L. Chen, A ternary B, N, P-doped carbon material with suppressed water splitting activity for high-energy aqueous supercapacitors, Carbon N. Y. 170 (2020) 127–136, https://doi.org/10.1016/j.carbon.2020.08.013.

[30] H. Rustamaji, T. Prakoso, H. Devianto, P. Widiatmoko, K.A. Kurnia, Facile synthesis of N, S-modified activated carbon from biomass residue for promising supercapacitor electrode applications, Bioresour. Technol. Rep. 21 (2023), https://doi.org/10.1016/j.biteb.2022.101301.

[31] H.V.T. Nguyen, K.K. Lee, Tailoring solvent mixtures to boost electrochemical stability and low-temperature performances of supercapacitors, J. Power Sources 592 (2024), https://doi.org/10.1016/j.jpowsour.2023.233929.

[32] J. Segalini, E. Iwama, P.L. Taberna, Y. Gogotsi, P. Simon, Steric effects in adsorption of ions from mixed electrolytes into microporous carbon, Electrochem. Commun. 15 (2012) 63–65, https://doi.org/10.1016/j.elecom.2011.11.023.

[33] W. Yi, S. Wu, Z. Zhou, X. Fang, X. Sun, J. Li, Low-cost "water-in-salt" hydrogel electrolyte enabled flexible supercapacitors with 2.7 V voltage and −40 °C adaptability, ACS Appl. Energy Mater. 6 (2023) 8838–8848, https://doi.org/10.1021/acsaem.3c01409.

[34] M. Huang, S. Zhen, X. Ren, X. Ju, High-voltage hydrous electrolytes for electrochemical energy storage, J. Power Sources 465 (2020), https://doi.org/10.1016/j.jpowsour.2020.228265.

[35] H.L. Wang, M.S. Kumar, H.X. Chang, M. Hulman, J.Y. Lin, Wide-potential, low-temperature supercapacitors enabled by dimethyl sulfoxide-based hybrid deep eutectic solvents, J. Taiwan Inst. Chem. Eng. 172 (2025), https://doi.org/10.1016/j.jtice.2025.106131.

[36] W. Yi, S. Wu, Z. Zhou, X. Fang, X. Sun, J. Li, Low-cost "water-in-salt" hydrogel electrolyte enabled flexible supercapacitors with 2.7 V voltage and −40 °C adaptability, ACS Appl. Energy Mater. 6 (2023) 8838–8848, https://doi.org/10.1021/acsaem.3c01409.

[37] K. Su, C. Wang, Y. Pu, Y. Wang, P. Ma, L. Liu, X. Tian, H. Du, J. Lang, Dilute aqueous hybrid electrolyte endows a high-voltage window for supercapacitors, J. Alloys Compd. 1002 (2024), https://doi.org/10.1016/j.jallcom.2024.175354.

[38] Z. Bo, X. Zhang, Z. Huang, Y. Huang, J. Yan, K. Cen, H. Yang, Binary ionic liquids hybrid electrolyte based supercapacitors with high energy & power density, RSC Adv. 13 (2023) 15762–15771, https://doi.org/10.1039/d3ra01634j.

[39] M. Pang, S. Jiang, J. Zhao, S. Zhang, R. Wang, N. Li, R. Liu, Q. Pan, W. Qu, B. Xing, "Water-in-salt" electrolyte enhanced high voltage aqueous supercapacitor with carbon electrodes derived from biomass waste-ground grain hulls, RSC Adv. 10 (2020) 35545–35556, https://doi.org/10.1039/d0ra07448a.

[40] W. Yi, S. Wu, Z. Zhou, X. Fang, X. Sun, J. Li, Low-cost "Water-in-Salt" hydrogel electrolyte enabled flexible supercapacitors with 2.7 V voltage and −40 °C adaptability, ACS Appl. Energy Mater. 6 (2023) 8838–8848, https://doi.org/10.1021/acsaem.3c01409.

[41] M. Pang, S. Jiang, J. Zhao, S. Zhang, R. Wang, N. Li, R. Liu, Q. Pan, W. Qu, B. Xing, "Water-in-salt" electrolyte enhanced high voltage aqueous supercapacitor with carbon electrodes derived from biomass waste-ground grain hulls, RSC Adv. 10 (2020) 35545–35556, https://doi.org/10.1039/d0ra07448a.